The 5th International Symposium - Supercritical CO2 Power Cycles
March 28-31, 2016, San Antonio, Texas

The influence of radiative transfer on the turbulent flow inside solar absorbers operating with supercritical CO_2

R. Pecnik *[1], S.H.H.J. Smit[1], A. Patel[1], and D.J.E.M. Roekaerts[1]

[1]Process and Energy Department, Delft University of Technology, Leeghwaterstraat 39, 2628 CB Delft, The Netherlands

1 Abstract

In this paper we investigate and compare two different solar receiver technologies for concentrated solar power plants operating with supercritical CO_2. The first receiver is based on conventional surface absorbers, while the second receiver is based on an innovative idea to use volumetric receivers where sunlight is transmitted through a transparent pipe and directly absorbed by nanoparticles dispersed in supercritical CO_2. The optical properties of the nanoparticles and the CO_2 at high pressures and temperatures have been first estimated and then used in a Navier-Stokes solver that has been coupled to a radiative transfer solver. The results indicate that for temperatures up to 700°C the volumetric receiver achieves thermal collector efficiencies up to 65% as compared to surface receivers with 50%.

2 Introduction

Sunlight has by far the highest potential of the Earth's renewable energy sources. Yet, the main challenges for the widespread adoption of solar power systems are their currently low conversion efficiency and high capital cost. To reduce the high capital cost and to increase the low overall efficiencies of current thermal solar power plants, two significant challenges must be overcome. First, the working fluids and heat carrier mediums, such as synthetic oils or molten salts, have a temperature limit of approximately 400C and 550C, respectively. When combined with a steam Rankine power cycle, the cycle efficiency is below 30%. Second, surface-based receivers, as shown in figure 1a, are not well suited for transferring heat to the fluid. In particular, a large temperature difference between the absorber surface and the fluid arises at high levels of solar concentration. This leads to significant emissive losses at the surface of the solar receiver with efficiencies of 55% for a typical application [1]. Accordingly, current solar fields are extremely large and very expensive [3]. As a result, the combined solar power plant conversion efficiency is below 20%.

The use of nanofluids in volumetric receivers, as shown in figure 1b, where nanoparticles in a liquid medium directly absorb solar radiation, potentially offers paradigm shift in harvesting solar energy. For instance, if the current technology is replaced with volumetric receivers, combined

*Electronic address: r.pecnik@tudelft.nl; Corresponding author

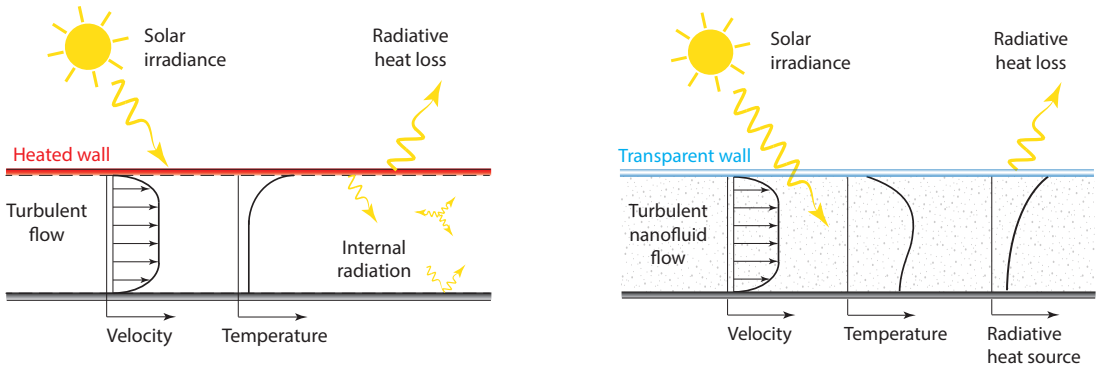

(a) Surface receiver: the upper plate captures concentrated sunlight and transfers heat to the fluid inside.

(b) Volumetric receiver: concentrated sunlight is transmitted through a transparent wall and directly irradiates nanoparticles within the fluid, which then transfer heat to the working fluid.

Figure 1: Surface vs. volumetric receiver.

with a supercritical CO_2 Brayton cycle, the total plant efficiency can potentially be increased to an unprecedented level of 35%. This technology would then outperform the competing renewable energy systems by means of cost-effectiveness and conversion efficiency.

The aim of this study is to numerically investigate the performance of a volumetric solar receiver operating with supercritical CO_2. Results for the two absorbers are presented and compared: a surface absorber with diffusively reflective and emitting wall, and a volumetric absorber with a transparent wall that has directionally dependent optical properties – transparent from outside and specularly reflective from inside the receiver if the radiation is within the critical angle. Both configurations are shown in figure 1. For both receivers the inlet temperature is set to 550°C (approximate recuperator outlet temperature of a closed loop supercritical CO_2 Brayton cycle) and the maximum outlet temperature is specified to 750°C. Efficiencies and temperature profiles are compared and analysed. The results indicate that the for all of the configurations tested the volumetric receiver outperforms the conventional surface by 10 to 15% efficiency points.

The paper is organized as follows. In section 3 we discuss the governing equations and the optical and thermophysical properties of the supercritical CO_2, the nanoparticles and the colliod. Section 4 briefly introduced the developed Navier-Stokes and the radiative solver that have been used in this work. The specific boundary conditions and investigated parameters are presented in section 5. Several parameters have been varied, such as the Reynolds number, solar concentration factor, surface emissivities, nanoparticle volume fraction, and the critical angle for which radiation can escape the inside of the volumetric receiver. The results are presented in section 6 and the work is concluded in section 7.

3 Governing equations

We use the Favre-averaged Navier-Stokes equations to solve the fluid flow within the channel. The conservation equations for mass, momentum and energy are given in the low-Mach number approximation of the Navier-Stokes equations as:

$$\frac{\partial \overline{\rho} \widetilde{u}_i}{\partial x_j} = 0, \tag{1}$$

$$\frac{\partial \overline{\rho}\widetilde{u}_i\widetilde{u}_j}{\partial x_j} = \frac{\partial \overline{p}_i}{\partial x_i} + \frac{1}{Re_0}\frac{\partial \overline{\tau}_{ij}}{\partial x_j}, \tag{2}$$

$$\frac{\partial \overline{\rho}\widetilde{h}\widetilde{u}_j}{\partial x_j} = \frac{\partial}{\partial x_j}\left[\left(\frac{\overline{\alpha}}{Re_0 Pr_0} + \frac{\mu_t}{Pr_t}\right)\frac{\partial \widetilde{h}}{\partial x_j}\right] - R\frac{\partial q_r}{\partial x_j}, \tag{3}$$

with the viscous stress tensor $\overline{\tau}_{ij} = 2\overline{\mu}_{eff}S_{ij} = \overline{\mu}_{eff}\left(\partial\widetilde{u}_i/\partial x_j + \partial\widetilde{u}_j/\partial x_i - 2/3\ \partial\widetilde{u}_k/\partial x_k\ \delta_{ij}\right)$ and $\alpha = k_c/c_p$, with k_c the thermal conductivity and c_p the isobaric heat capacity $c_p = dh/dT|_p$. $\overline{\rho}$ is the density of the fluid (nanofluid), $\overline{u}_i$ the velocity, $\widetilde{h}$ the enthalpy and $\overline{\mu}_{eff} = \overline{\mu} + \mu_t$ is the effective viscosity (sum of molecular and turbulent viscosity). The bar ($^-$) and the tilde ($\tilde{}$) indicate Reynolds-averaged and Favre-averaged quantities, respectively, which appear due to turbulence modelling. The non-dimensional parameters are the Reynolds and Prandtl number, and $R = CG_sH/(T_0k_{c0})$ with C is the solar concentration factor, G_s the solar radiative heat flux (assumed to be 1000 W/m^2) and H the receiver height. The subscript 0 indicates reference conditions at the inlet of the heated channel.

with the viscous stress tensor $\overline{\tau}_{ij} = 2\overline{\mu}_{eff}S_{ij} = \overline{\mu}_{eff}\left(\partial\widetilde{u}_i/\partial x_j + \partial\widetilde{u}_j/\partial x_i - 2/3\ \partial\widetilde{u}_k/\partial x_k\ \delta_{ij}\right)$ and $\alpha = k_c/c_p$, with k_c the thermal conductivity and c_p the isobaric heat capacity $c_p = dh/dT|_p$. $\overline{\rho}$ is the density of the fluid (nanofluid), $\overline{u}_i$ the velocity, $\widetilde{h}$ the enthalpy and $\overline{\mu}_{eff} = \overline{\mu} + \mu_t$ is the effective viscosity (sum of molecular and turbulent viscosity). The bar ($^-$) and the tilde ($\tilde{}$) and Reynolds-averaged and Favre-averaged quantities, respectively, which appear due to turbulence modelling. The non-dimensional parameters are the Reynolds and Prandtl number, and $R = CG_sH/(T_0k_{c0})$ with C is the solar concentration factor, G_s the solar radiative heat flux (assumed to be 1000 W/m^2) and H the receiver height. The subscript 0 indicated reference conditions at the inlet of the heated channel.

The radiative heat source term in equation 3 is given as:

$$\frac{\partial q_r}{\partial x_j} = \int_0^\infty \kappa_\lambda \left(4\pi I_{b\lambda} - \int_{4\pi} I_\lambda d\Omega\right) d\lambda, \tag{4}$$

whereby the radiative intensity I_λ can be obtained by the general spectrally integrated radiative transfer equation (RTE),

$$\int_0^\infty \frac{dI_\lambda}{ds} d\lambda = \int_0^\infty \kappa_\lambda (I_{b\lambda} - I_\lambda) d\lambda \tag{5}$$

where κ_λ is the absorption coefficient and $I_{b\lambda}$ is the blackbody radiation. Note, the given radiative transfer equation is for a non-scattering medium. The reason for this will be explained later.

3.1 Thermophysical properties

The pressure of the supercritical CO_2 in the receiver is set to 200 bar and assumed to be constant. Thus the transport properties are only a function of the temperature. The properties of CO_2 are taken from RefProp [5] and their distributions within a temperature range of 500 to 1700 °C are shown in figure 2. For the case of the volumetric receiver with the nanofluid as a heat transfer medium the thermophysical properties can be taken to be equal to the basefluid [6]; supercritical CO_2 in this case. The turbulent viscosity μ_t is obtained by solving the $k-\epsilon$ turbulence model of Myong and Kasagi [9].

3.2 Optical properties

The optical properties of the fluid are not readily available in literature. First the optical properties for CO_2 are extrapolated to high pressure and temperature and the optical properties of the nanoparticles are calculated. Those are then combined to obtain the properties for the nanofluid.

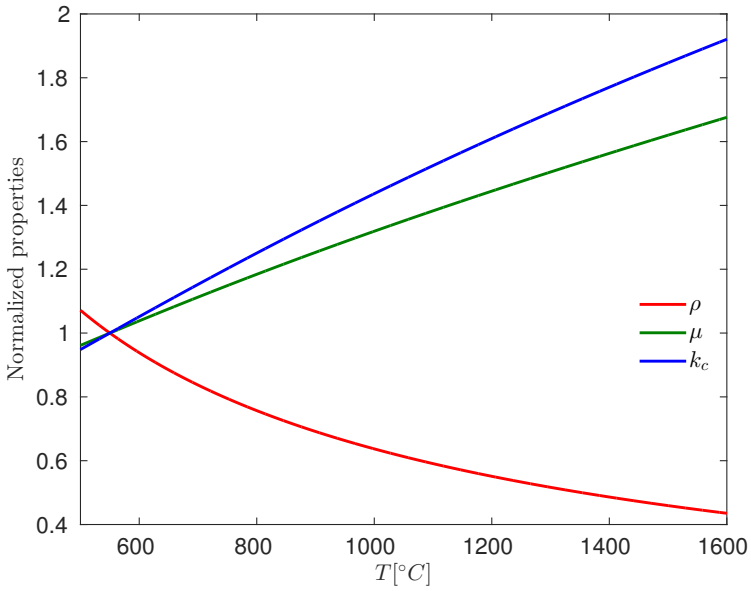

Figure 2: Normalized thermophysical properties of CO_2 at 200 bar. The reference values for the normalization are taken at 550°C, where the properties are: density $\rho_0 = 124.4$ [kg/m^3], dynamic viscosity $\mu_0 = 3.74e-05$ [Pa s] and thermal conductivity $k_0 = 0.062$ [W/m/K].

sCO2 The optical properties of pure CO_2 are calculated with high definition spectral data from the HITEMP [15] database, by means of Lorentz broadening, corrected for the sub-Lorentzian behaviour using empirical-fitted parameters [13]. An adjusted version of the open-source software *k-spectrum* [2] is used for the broadening calculations. The Lorentz curve used to broaden the spectral lines is given by equation 6.

$$\kappa_{\nu,j} = \rho^2 \frac{S_j}{\pi} \frac{\nu}{\nu_0} \frac{\gamma_c}{(\nu - \nu_{0,j})^2} \chi\left((\nu - \nu_0), T\right) \tag{6}$$

The results of the simulation for the the absorption spectra of CO_2 at a pressure of 200 bar for different temperatures are depicted in figure 3. The CO_2 is optically thick in three wavelength bands with peaks at approximately 3, 4.5, and 15 μm, and optically thin in most part of the remaining spectrum.

Nanoparticles For practical applications it is essential to use cost-effective, but highly absorbing nanoparticles. For this reason we chose Copper and Nickel nanoparticles, which have a high extinction coefficient in the visible light spectrum [16]. The required optical properties of Copper and Nickel are taken from literature [14, 10]. Figure 4a shows the results of the combined data for the index of refraction n and index of absorption k. Pressure and temperature dependencies have not been taken into account for the optical property of the nanoparticles.

The properties of copper particles – index of refraction and absorption – are then used in the Rayleigh scattering approximation [7] to determine the absorption due to the presence of particles in the basefluid, as

$$\kappa_\lambda = -\Im\left(\frac{m^2 - 1}{m^2 + 2}\right) \frac{6\pi\phi}{\lambda}. \tag{7}$$

Figure 4b shows the optical properties of copper particles as a function of the wavelength, calculated with the Rayleigh scattering theory and properties from the literature. Different volume fractions

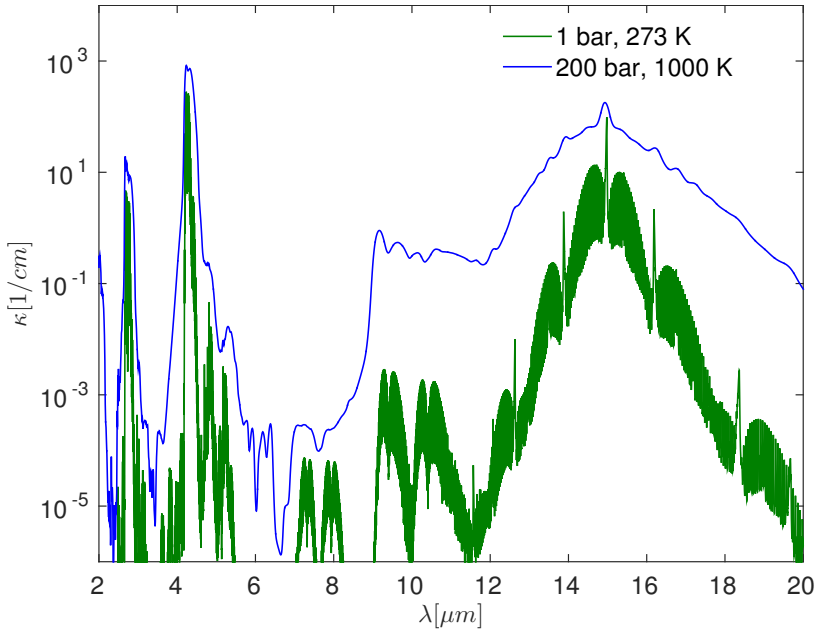

Figure 3: Absorption coefficient of CO_2 as a function of the wavelength at 200 bar with varying temperature

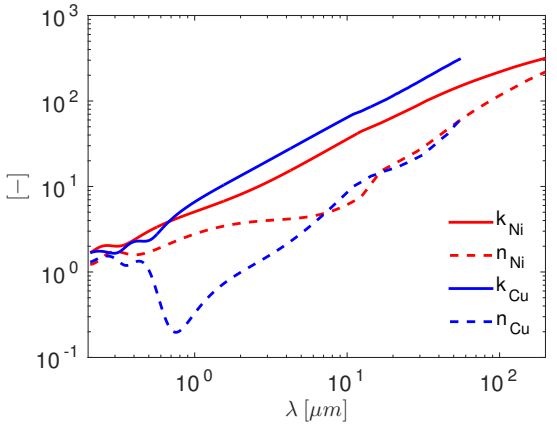

(a) Index of refraction and absorption (merged datasets of Rakić et al. [14] and Ordal et al. [10])

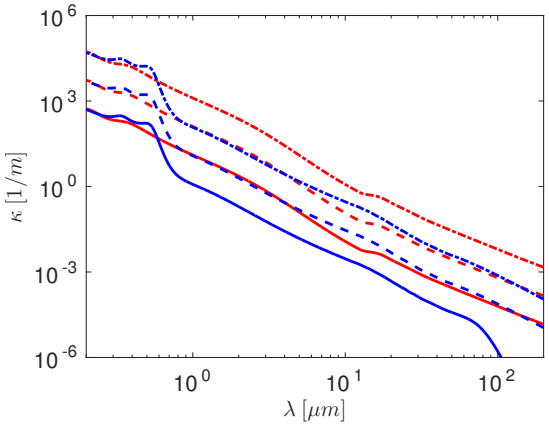

(b) Absorption coefficient particle clouds: (——) $\phi = 1 \cdot 10^{-5}$, (– – –) $\phi = 1 \cdot 10^{-4}$, (—·—) $\phi = 1 \cdot 10^{-3}$

Figure 4: Optical properties of Nickel (red) and Copper (blue)

of nanoparticles have been used to show the effect on the absorption coefficient. It is clearly visible that the absorption coefficient increases with a higher volume fraction. For larger wavelengths the absorption coefficient will approach zero. This means that the absorber can be optimized by varying the volume fraction of the nanofluid, as this will only effect the optical thickness within the solar spectrum.

Nanofluid The resulting absorption coefficient of the nanofluid is calculated by adding the absorption coefficients of the sCO_2 and the particles. This is a reasonable approximation as the absorption coefficient of the sCO_2 is large where the absorption coefficient of the nanoparticles

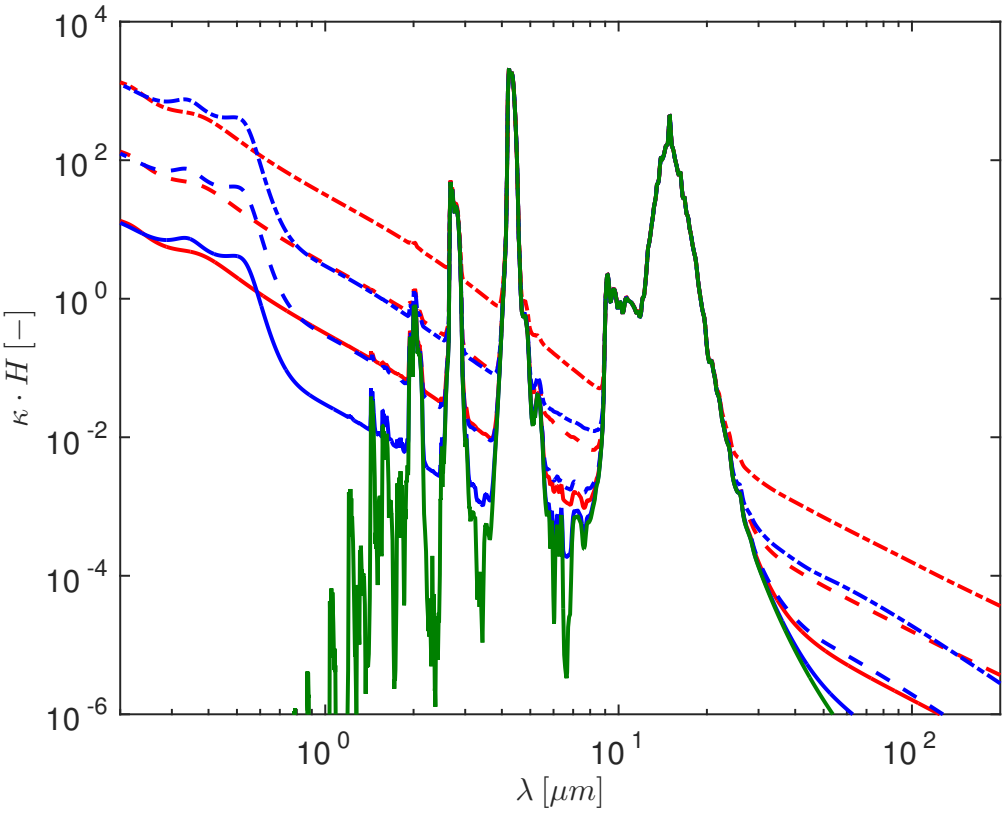

Figure 5: Absorption spectra of nanofluid as a function of the wavelength η at a temperature of 1000 K and pressure of 200 bar. Optical properties of sCO_2-Nickel (red) and sCO_2-Copper (blue), pure sCO_2 (green). Nanoparticle volume fractions: (——) $\phi = 1 \cdot 10^{-5}$, (– – –) $\phi = 1 \cdot 10^{-4}$, (—·—) $\phi = 1 \cdot 10^{-3}$.

is small and vice versa. Thus, the combined absorption of the nanofluid is a linear combination (simplified effective medium theory) of the base fluid and the nanoparticles [16], as

$$\kappa_{nf} = \kappa_p + \kappa_f. \tag{8}$$

The absorption spectra for the nanofluid are given in figure 5. Additionally, the fraction of black-body energy is depicted for two different emission temperatures, one at the surface temperature of the sun (5800 K), and one for the emission temperature as expected in the absorber (1000 K). This clearly demonstrates that the re-emitted radiation of the nanofluid is attenuated by the sCO_2, while the solar radiation is absorbed by the nanoparticles.

Moreover the change in the absorption spectra due to the change in volume fraction is entirely due to the absorption of the particles. This is because of the simplified effective medium theory, which assumes that there is no interaction between the absorption of the particles and the basefluid. Therefore, the volume fraction of the particles is not affecting the absorption of the sCO_2.

4 Numerical method

4.1 Navier-Stokes solver

The Reynolds-averaged Navier-Stokes equations are solved using a staggered arrangement of the velocity on a cartesian two-dimensional grid. The scalar equations (enthalpy h, turbulent kinetic energy k and turbulent dissipation rate ϵ) are discretized at the cell center, whereas the momentum equations are discretized at the velocity points, which are located at the cell face. A second order central differencing scheme is used to discretize the spatial derivatives and the Semi-Implicit Method for Pressure Linked Equations (SIMPLE) is used to obtain the steady state solution. The code has been extensively validated for supercritical heat transfer simulations in Patel [12].

4.2 Radiative transfer solver

4.2.1 Finite Volume Method

To solve the radiative transfer equation (equations (5) and (4)) numerically, the Finite Volume Method (FVM) is used as presented by Modest [7]. The solid angle Ω is divided into i parts by discretizing the polar angle θ, and the azimuthal angle ψ. The corresponding directional vectors $\boldsymbol{s}_i$, for each discrete solid angle Ω_i, can then be calculated by integrating the directional vector $\hat{\boldsymbol{s}}$ over the discretization of the solid angle:

$$\Omega_i = \int_{\Omega_i} d\Omega \;\; = \int_{\Delta\psi_i}\int_{\Delta\theta_i} sin\,\theta\, d\theta d\psi \tag{9}$$

$$\boldsymbol{s}_i = \int_{\Omega_i} \hat{\boldsymbol{s}} d\Omega = \int_{\Delta\psi_i}\int_{\Delta\theta_i} (sin\,\theta\, cos\,\psi\, \hat{\boldsymbol{i}} + sin\,\theta\, sin\,\psi\, \hat{\boldsymbol{j}} + cos\,\theta\, \hat{\boldsymbol{k}}) sin\,\theta\, d\theta d\psi. \tag{10}$$

A volume balance is made over a two-dimensional control volume by using the directional vectors $\boldsymbol{s}_i$, the discrete solid angles Ω_i. Additionally the wavelength spectrum is discretized, such that the absorption coefficient κ_λ for each discrete portion of the wavelength spectrum $\Delta\lambda_j$,

The absorption coefficient

the absorption coefficient κ_λ can be taken to be constant

equation (4) and (5) are transformed into:

A volume balance is made over a two-dimensional control volume, while using the directional vectors $\boldsymbol{s}_i$, the discrete solid angles Ω_i, and discretizing the wavelength spectrum in j pieces equation (4) and (5) are transformed into:

$$\sum_j^M \left(|\boldsymbol{s}_i \cdot \hat{\boldsymbol{i}}| \frac{\partial I_{i,j}}{dx} + |\boldsymbol{s}_i \cdot \hat{\boldsymbol{j}}| \frac{\partial I_{i,j}}{dy} + \kappa_j I_{i,j} \Omega_i \right) = \sum_j^M \kappa_j I_{b,j} \Omega_i, \tag{11}$$

$$\nabla q_{rad} = \sum_j^M \left(\kappa_j \left(4\pi I_{b,j} - \sum_i^N I_{i,j} \Omega_i \right) \right), \tag{12}$$

where $I_{b,j} = \int_{\Delta\lambda_j} I_{b,\lambda} d\lambda$.

The direct discretization of the spectrum into j parts is not recommended because the absorption coefficient κ_λ is wildly varying across the spectrum. For an accurate discretization of the spectrum one thus needs a lot of discrete portions $\Delta\lambda_j$. To solve this problem a weighted-sum-of-grey-gasses is used, where instead of fitting the absorption coefficient directly, transformations are made so that the absorption coefficient can be accurately fitted with less parameters. This will be discussed in the next section.

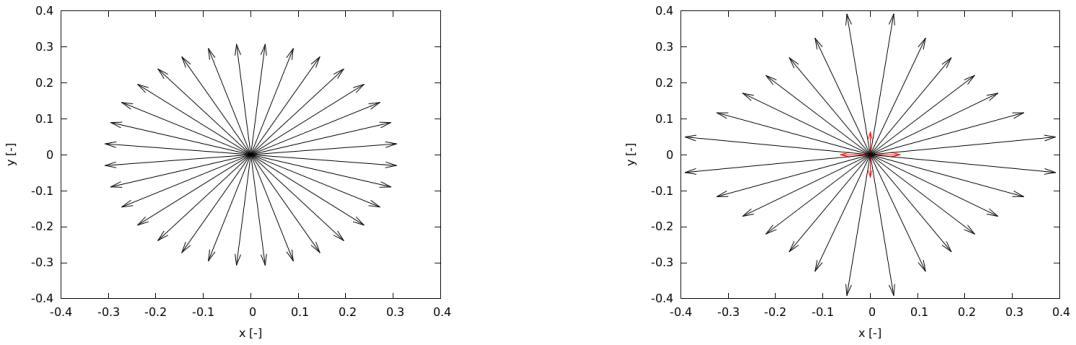

(a) Standard equidistant grid

(b) Adjusted grid

Figure 6: The two angular grids with $N = 32$

Angular grids In this paper two angular grids are used. One standard angular grid, which is used for the surface absorber, and one adjusted angular grid for the volumetric absorber, shown in figure 6. The reason for changing the grid is related to the collimated radiation. For the surface absorber, the collimated radiation is absorbed by the surface so the boundary conditions for the radiation inside the absorber have no directional dependency —assuming isotropic emission and reflectance of the plate. However, for the volumetric absorber the boundary conditions are non isotropic as the collimated radiation of the sun is used as the boundary condition. Therefore the RTE for the volumetric solar receiver is solved using an angular grid, which includes the direction of the collimated radiation. The number of directions is chosen such that the solution is grid independent.

4.2.2 Weighted-sum of grey gasses model

To incorporate the non-grey radiative properties the weighted-sum-of-grey-gasses (WSGG) is used as presented by Modest and Zhang [8]. In the article they showed that an approximation of their full k-distribution model –a model which transforms the RTE from wavelength space to k-space– can be reduced to the WSGG model. The full k-distribution model makes use of the fact that for different wavelengths the same absorption coefficient exists. By transforming the RTE from wavelength space to k-space, these wavelengths are matched in order to reduce the number of equations for which the RTE has to be solved. Equations (11) and (12) can then be transformed using the WSGG formulation to,

$$\sum_{n=1}^{G}\left(|\boldsymbol{s}_i\cdot\hat{\boldsymbol{i}}|\frac{\partial I_{i,n}}{dx}+|\boldsymbol{s}_i\cdot\hat{\boldsymbol{j}}|\frac{\partial I_{i,n}}{dy}+K_nI_{i,n}\Omega_i\right)=\sum_{n=1}^{G}K_nA_nI_b\Omega_i, \tag{13}$$

$$\nabla q_r=\sum_{n=1}^{G}\nabla q_{r,n}=\sum_{n=1}^{G}K_n\left(4\pi A_nI_b-\sum_i I_{i,n}\Omega_i\right), \tag{14}$$

where G is the total number of grey gasses, K_n is the fitted absorption coefficient and A_nI_b is the weighted emission of black body radiation. It is assumed that the radiative properties are independent of temperature. The distributions are approximated by 9 grey gasses, where a genetic algorithm has been used to minimize the approximation error.

Two different k-distributions are approximated for the volumetric absorber. This can be done because the directions are independent from each other due to the assumption of a non-scattering

medium. The approximated k-distribution for the direction of the collimated radiation has an emission reference temperature of 5800 K and the distribution for the other directions has an emission reference temperature of 1000 K. This enables us to directly approximate the most relevant k-distribution for each direction.

5 Simulation cases

5.1 Surface receiver model

The surface absorber consists of a coated plate that has a high emissivity in the visual light spectrum and a low emissivity outside this spectrum to ensure that as little as possible heat is lost to the environment. The following assumptions are made in this study:

- diffusively reflective rear- and front side of the plate;
- step-wise emissivity for the front side of the plate (side subjected to the solar radiation): emissivity $\epsilon_{f,1} = 0.9$ for wavelengths below the wavelength limit $\lambda_{lim} = 2\mu m$ and $\epsilon_{f,2} = 0.1$ above;
- constant emissivity for the rear side of the plate ϵ_b;
- and no convective heat transfer from the wall to the surroundings is modelled, which is applicable for vacuum-pipe collectors.

To investigate the effect of neglecting the radiative heat transfer, also cases without radiative heat transfer are simulated. In table 1b the studied parameters for the surface receiver are given.

5.2 Volumetric receiver model

The volumetric absorber consists of a transparent glass plate, such that the light solar light is transmitted into the receiver and absorbed by the dispersed nanoparticles. The following assumptions are made with regard to the volumetric solar receiver:

- directional dependent specular reflective top: radiation hitting the transparent plate can pass without getting absorbed if its angle is smaller than the critical angle δ_c. If the angle is larger than the critical angle it is specular reflective;
- the critical angle δ_c is assumed to be constant over the wavelength λ;
- and – as for the surface receiver – no convective heat transfer from the wall to the surroundings is modelled.

The volumetric receiver is characterized by the critical angle and the volume fraction of nanoparticles. In table 1b the parameter values for the the volumetric receiver are given.

Re	5000, 7000, 9000
C	30, 50, 70

(a) General

Surface		Volumetric	
ϵ	0.0, 0.5, 1.0	ϕ	$1 \cdot 10^4$, $2 \cdot 10^4$, $3 \cdot 10^4$
		δ_c	30, 50, 70

(b) Receiver specific

Table 1: Parameter space for the simulations

5.3 Boundary conditions and investigated parameters

The the inlet temperature T_{in} for both receivers is taken to be 550°C and the desired temperature increase corresponds to $\Delta T = 200$°C. The temperatures have been chosen such that the receiver can operate as a superheater in a closed loop sCO_2 Brayton-cycle as given in Iverson et al. [4]. The height of the channel is taken to be 2.5 cm and the Prandtl number is 0.742. Several Reynolds numbers and solar concentration factors have been simulated, summarized in table 1a.

6 Results

In order to compare the performance of both receivers, the efficiency is computed as a function of the stream wise coordinate as follows

$$\eta_{rec,x} = \frac{\dot{m}(h_x - h_{in})}{q_s A_{rec,x}}, \tag{15}$$

where h_x is the bulk enthalpy at a given stream wise distance x, $\dot{m}$ the mass flux, h_{in} the inlet enthalpy, q_s the total incoming solar energy per unit length, and $A_{rec,x}$ is the receiver area.

6.1 Surface receiver

The stream wise distributions for the bulk temperature and receiver plate temperature are discussed in figure 7a and 7b, repectively, for different back-side emissivities ϵ_b and for three solar concentration factors. The solutions without the radiative heat transfer are also shown. The increase of bulk temperature is larger for higher backside emissivities and it is the lowest when the radiative heat transfer is not taken into account. This effect is more pronounced for larger solar concentration factors. For example, the difference between the solutions with and without radiation modelling inside the receiver can reach up to 35°C for the bulk temperature at the outlet of the receiver. This can be explained by the high absorption coefficient of CO_2 at 200 bar above a wavelength of 9 μm (see figure 3). On the other hand, if the radiation inside the surface receiver is taken into account, the receiver plate temperature significantly decreases (figure 7b). The lowest wall temperature is obtained with the highest emissivity.

6.2 Volumetric receiver

Figure 8 shows temperature profiles for the volumetric receiver at different stream wise locations, whereby the effect of nanoparticle volume fraction is given in figure 8a and the effect of different critical angles is given in figure 8b. At the beginning of the absorber (red) the increase of volume fraction leads to higher temperatures at the transparent wall and to lower temperatures at other side. This is expected, as with higher volume fractions the nanofluid is optically thick and thus absorbs the entire sunlight in a thin layer close to the transparent wall. On the other hand, the temperature profile is more uniform for low values of nanoparticle volume fractions.

Also the critical angle (the angle at which radiation can escape the receiver) has a large influence on the temperature profile. The smaller the critical angle the higher the temperatures in the receiver. This is because less radiation can escape and more is specularly reflected by the transparent plate. The difference between the temperatures is larger towards the outlet of the receiver.

Receiver efficiency as a function of volume fraction is plotted in figure 9. The solar concentration factor in this plot is set to 75. It can be seen that, independent of the receiver outlet temperature, the maximum efficiency is obtained for a volume fraction of $\phi = 4 \cdot 10^{-5}$.

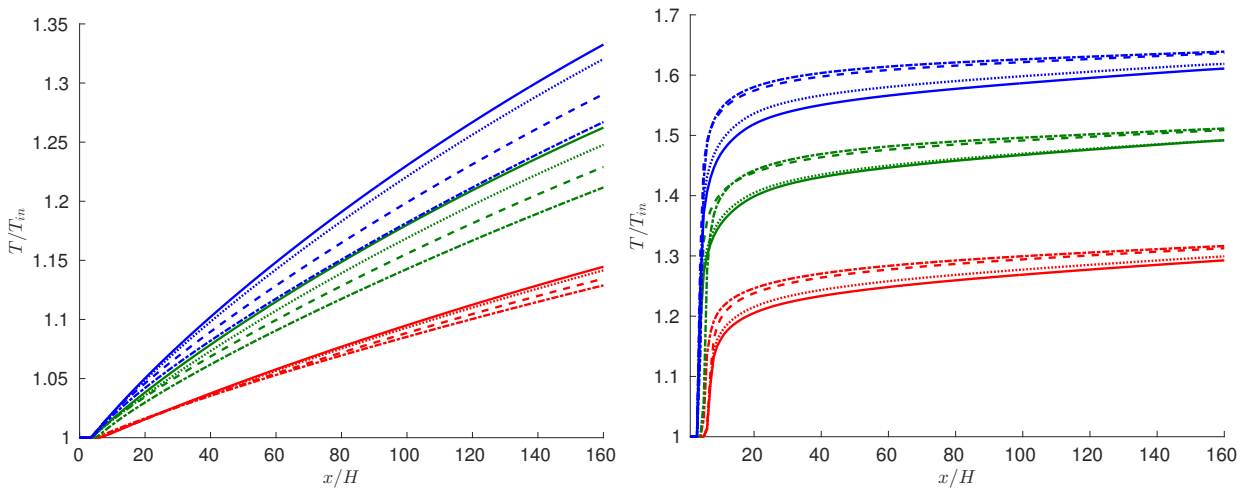

(a) Bulk temperature

(b) Receiver plate temperature

Figure 7: Surface receiver: (——) $\epsilon_b = 1$, (·····) $\epsilon_b = 0.5$, (– – –) $\epsilon_b = 0.0$ and (—·—) no radiative heat transfer; C=75 (blue), C=50 (green), C=25 (red).

6.3 Volumetric versus surface receiver

In figure 10 contour plots are given for the surface and volumetric receiver. The solar concentration factor is 50 for both cases. The backside emissivity is 1 for the surface receiver and the volume fraction is $2 \cdot 10^{-4}$ for the volumetric receiver. By comparing the temperature contours of the surface (figure 10a) and the volumetric receiver (figure 10b), it is apparent that the temperature increase is more homogeneous for the volumetric receiver, while the surface receiver shows typical profiles with high temperatures at the hot wall. Due to the homogeneous temperature increase in the volumetric receiver the velocity is more a symmetric than the volumetric receiver (figure 10d).

Temperature profiles at three different stream wise locations for both receivers are shown in figure 11. Once more, it is clearly visible that the temperature gradient for he surface receiver is much larger than for the volumetric receiver. As expected, the temperature gradient increases with increasing concentration factor. The volumetric receiver shows much smoother temperature profiles. The higher the solar concentration factor, the stronger the volumetric heating.

The bulk stream wise temperature and efficiency distributions for the surface and volumetric receivers are compared with each other in figure 12a for different solar concentration ratios and different Reynolds numbers. On can see that for low solar concentrations the difference in bulk temperature between the surface receiver and the volumetric receiver is small whereas this difference increases with higher solar concentration factors. Interestingly, the efficiency of the surface receiver is decreasing with higher solar concentration factors, whereas the efficiency of the volumetric receiver is increasing. The effect of the Reynolds number on the thermal receiver efficiency is plotted in figure 13. Based on the simulations the Reynolds number has a small effect on the efficiency for the volumetric receiver, while the surface receiver efficiency increases with increasing Reynolds number.

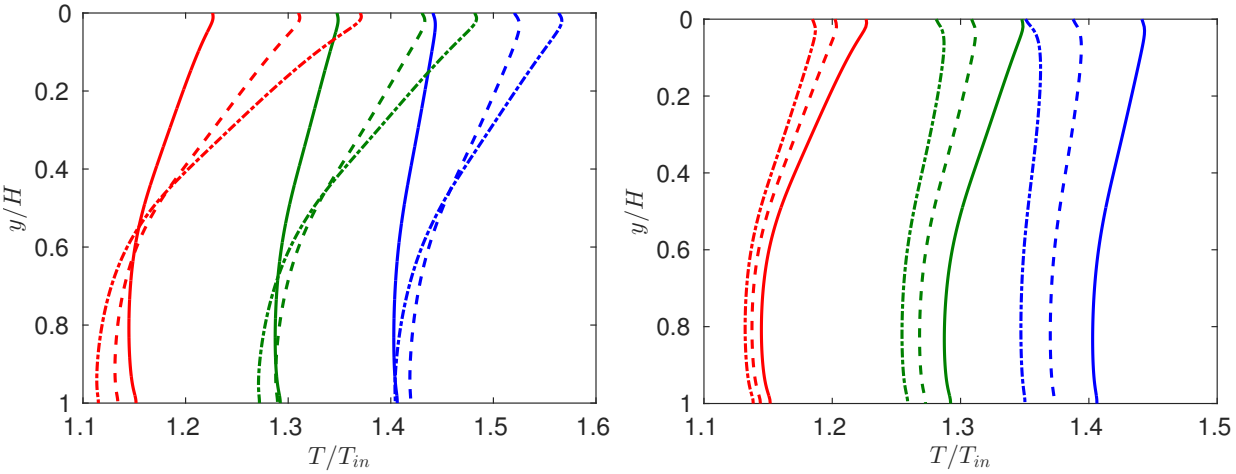

(a) Effect of volume fraction: (——) $\phi = 1 \cdot 10^{-4}$, (– – –) $\phi = 2 \cdot 10^{-4}$, (—-—) $\phi = 3 \cdot 10^{-4}$

(b) Effect of critical angle: (——) $\delta_c = 30°$, (– – –) $\delta_c = 50°$, (—-—) $\delta_c = 70°$

Figure 8: Transverse contour lines for volumetric absorber with C=50: $x/H = 50$ (red), $x/H = 100$ (green), $x/H = 150$ (blue)

7 Conclusion and recommendations

In this work we investigated two different concentrated solar receiver technologies that can be used to capture sunlight for a solar thermal power plant based on a recuperated closed loop supercritical CO_2 Brayton cycle. The receiver configurations are a conventional surface based absorber and a volumetric absorber based on nanofluids. By adding a small amount of nanoparticles to a basefluid – in this case supercritical CO_2 – the optical properties can be tuned to efficiently absorb solar radiation. Copper nanoparticles were chosen in this work, which have a high melting temperature and favourable optical properties within the solar spectrum.

In order to simulate these configurations, a Navier-Stokes code has been coupled to a radiative transfer solver. Both tools have been developed inhouse and validated for several benchmark cases (not shown). The optical properties of the supercritical CO_2 and the nanoparticles have been estimated at high pressure and temperatures. The weighted-sum-of-grey-gasses has been used to incorporate varying spectral properties in the radiative transfer equation.

For both receivers, several parameters have been varied, such as the Reynolds number, solar concentration factor, surface emissivities, nanoparticle volume fraction, and the critical angle for which radiation can escape the inside of the volumetric receiver. The numerical simulations showed that volumetric receivers have substantially higher efficiencies for high solar concentration factors. The radiative losses are lower, because of the low surface temperature as compared to the surface receiver. In order to further optimize the volumetric receiver, the volume fraction of nanoparticles can be used to tailor the absorption over the height of the absorber.

This study clearly indicates the superior receiver efficiency for volumetric receivers for high solar concentration factors. However, the caveat of this study lies in the limited knowledge of dispersed metal nanoparticles in supercritical CO_2. Although, nanoparticles do not have significant sedimentation velocities, do not cause significant erosion to the equipment, and do not readily deposit on walls, it is not clear what the nanoparticle agglomeration rate and nanoparticle stability will be in such a base fluid. Several studies are available in open literature that use supercritial fluids to synthesize or mix different nanoparticles. However, a detailed experimental characterization is

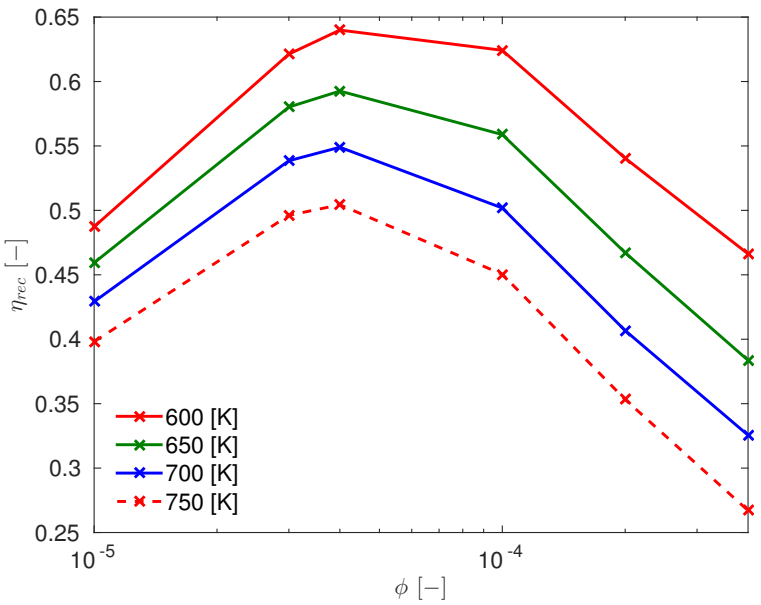

Figure 9: Receiver efficiency as a function of volume fraction for different receiver bulk outlet temperatures at Re=5000, with $\delta_c = 50°$ and $C = 75$.

required to ensure the viability of the proposed volumetric receiver concept of this work.

References

[1] G. Bakos, I. Ioannidis, N. Tsagas, and I. Seftelis. Design, optimisation and conversion-efficiency determination of a line-focus parabolic-trough solar-collector (ptc). *Applied energy*, 68(1):43–50, 2001.

[2] V. Eymet. kspectrum software, 2015. URL `something`.

[3] U. Herrmann, B. Kelly, and H. Price. Two-tank molten salt storage for parabolic trough solar power plants. *Energy*, 29(5):883–893, 2004.

[4] B. D. Iverson, T. M. Conboy, J. J. Pasch, and A. M. Kruizenga. Supercritical co 2 brayton cycles for solar-thermal energy. *Applied Energy*, 111:957–970, 2013.

[5] E. W. Lemmon, M. L. Huber, and M. O. McLinden. NIST Standard ReferenceDatabase 23: Reference Fluid Thermodynamic and Transport Properties - REFPROP. 9.0., 2010. URL `http://nist.gov/srd/nist23.cfm`.

[6] A. Lenert, Y. Zuniga, and E. Wang. Nanofluid-based absorbers for high temperature direct solar collectors. page 22208, 2010. IHTC14.

[7] M. F. Modest. *Radiative heat transfer*. Academic press, 2013.

[8] M. F. Modest and H. Zhang. The full-spectrum correlated-k distribution for thermal radiation from molecular gas-particulate mixtures. *Journal of heat transfer*, 124(1):30–38, 2002.

[9] H. K. Myong and N. Kasagi. A new approach to the improvement of k-epsilon turbulence model for wall-bounded shear flows. *JSME International Journal*, 33:63–72, 1990.

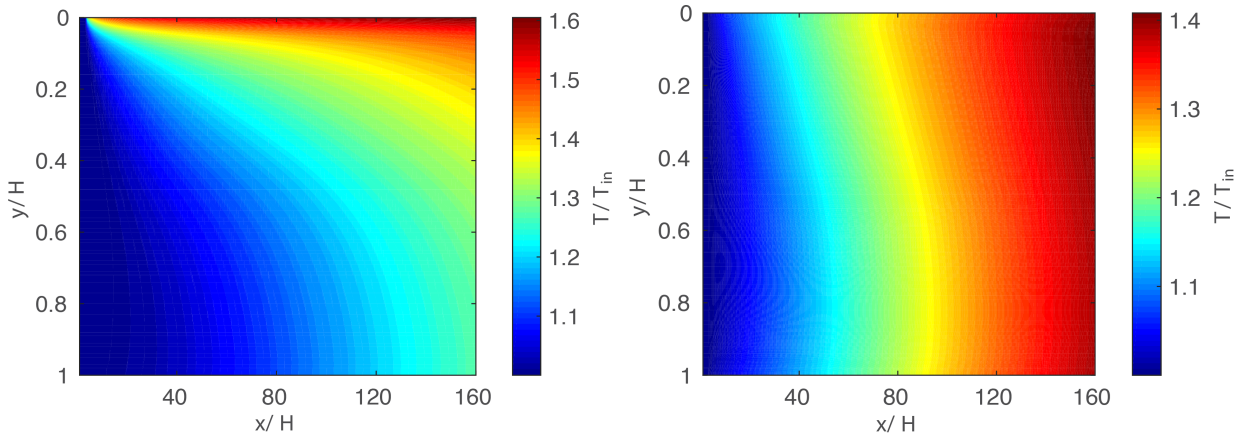

(a) Surface receiver: temperature

(b) Volumetric receiver: temperature

(c) Surface receiver: streamwise velocity

(d) Volumetric receiver: streamwise velocity

Figure 10: Contour plots of the surface and volumetric receiver

[10] M. A. Ordal, R. J. Bell, R. W. Alexander, L. L. Long, and M. R. Querry. Optical properties of fourteen metals in the infrared and far infrared: Al, co, cu, au, fe, pb, mo, ni, pd, pt, ag, ti, v, and w. *Appl. Opt.*, 24(24):4493–4499, Dec 1985.

[11] E. Palik. Handbook of optical constants of solids. 1998.

[12] A. Patel. Turbulence modeling for heat transfer to supercritical pipe flows. Master's thesis, TU Delft, Delft University of Technology, 2013.

[13] M. Perrin and J. Hartmann. Temperature-dependent measurements and modeling of absorption by co 2-n 2 mixtures in the far line-wings of the 4.3 μm co 2 band. *Journal of Quantitative Spectroscopy and Radiative Transfer*, 42(4):311–317, 1989.

[14] A. D. Rakić, A. B. Djurišić, J. M. Elazar, and M. L. Majewski. Optical properties of metallic films for vertical-cavity optoelectronic devices. *Appl. Opt.*, 37(22):5271–5283, Aug 1998. doi: 10.1364/AO.37.005271. URL `http://ao.osa.org/abstract.cfm?URI=ao-37-22-5271`.

[15] L. Rothman, I. Gordon, R. Barber, H. Dothe, R. Gamache, A. Goldman, V. Perevalov,

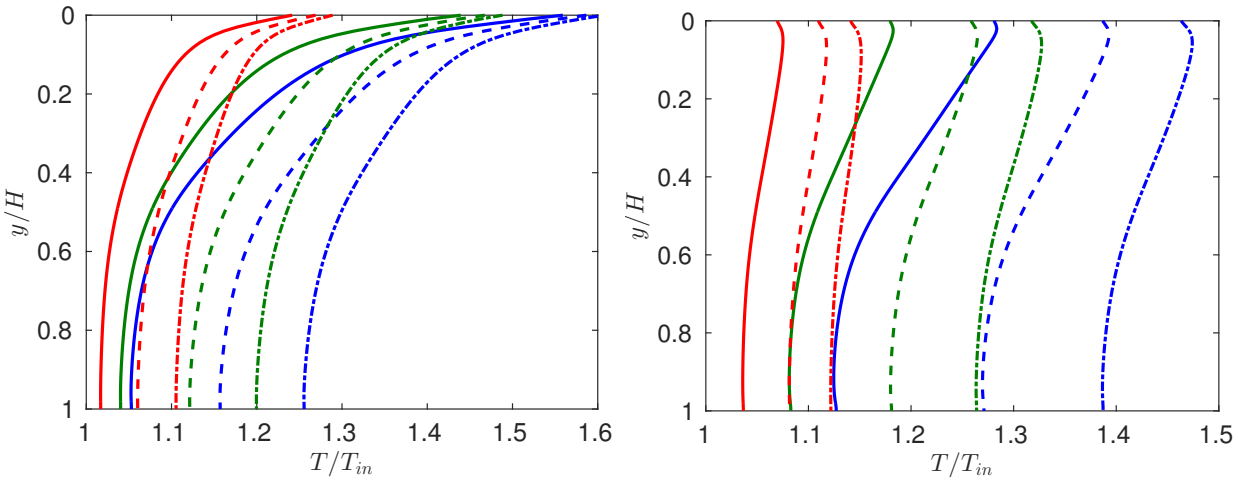

(a) Surface receiver: $\epsilon_b = 1$ (b) Volume receiver: $\delta_c = 50°$, $\phi = 2 \cdot 10^{-4}$

Figure 11: Transverse contourlines for C=25 (red), C=50 (green) and C=75 (blue): (——) x/H=50, (– – –) x/H=100, (—·—) x/H=160

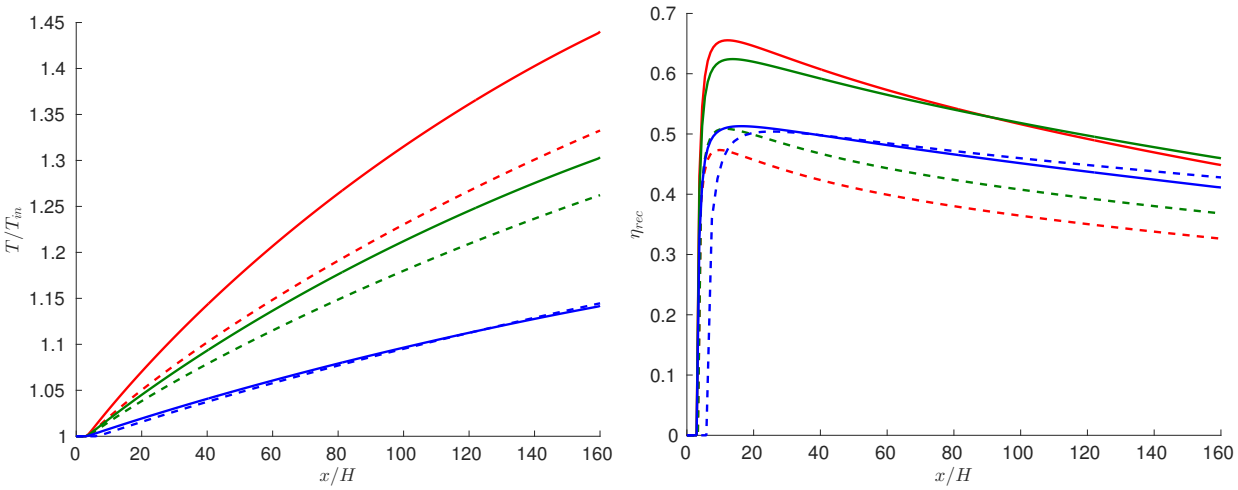

(a) Bulk temperature (b) Efficiency

Figure 12: (——) Volumetric receiver [$\delta_c = 50°, \phi = 2 \cdot 10^{-4}$] and (– – –) surface receiver [$\epsilon_b = 1$]: C=25 (blue), C=50 (green), C=75

S. Tashkun, and J. Tennyson. Hitemp, the high-temperature molecular spectroscopic database. *Journal of Quantitative Spectroscopy and Radiative Transfer*, 111(15):2139–2150, 2010.

[16] R. Taylor, P. Phelan, T. Otanicar, R. Adrian, and R. Prasher. Nanofluid optical property characterization: towards efficient direct absorption solar collectors. *Nanoscale Research Letters*, 6(1):225, 2011. ISSN 1556-276X. doi: 10.1186/1556-276X-6-225. URL `http://www.nanoscalereslett.com/content/6/1/225`.

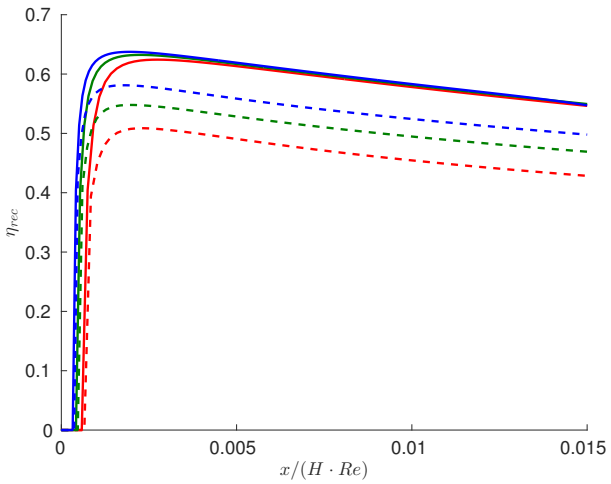

Figure 13: (——) Volumetric receiver $[\delta_c = 50°, \phi = 2 \cdot 10^{-4}]$ and (– – –) surface receiver $[\epsilon_b = 1]$: Re=5000 (red), Re=7000 (green) and Re=9000 (blue)

Biographies

Rene Pecnik, Dr. is an associate professor at Delft University of Technology, The Netherlands. His background is on high-fidelity fluid dynamic simulations for emerging renewable energy systems. He has received his doctoral degree from Graz University of Technology, Austria in 2007. From 2007 to 2010 he has been a postdoctoral fellow at the Center for Turbulence Research, Stanford University.

Stephan H. H. J. Smit is a MSc student at Delft University of Technology, The Netherlands. The topic of his graduation project is on volumetric solar receivers using nanofluids. The work presented in this manuscript is based on his investigations.

Ashish Patel, Ir. is a PhD student at Delft University of Technology, The Netherlands. His background is on turbulence research for real gas fluids with strong thermophysical variations.

Dirk J. E. M. Roekaerts, Dr. is an professor at Delft University of Technology, The Netherlands. His background is on reactive flows, turbulent combustion and radiative heat transfer. He received his PhD at the University Leuven, Belgium, in 1981. After several positions in industry and academia, he became professor for reactive flows Delft University of Technology in 2005.